

Impact of eccentricity on the population properties of neutron star – black hole mergers

GONZALO MORRAS ^{1,2}, GERAINT PRATTEN ³, AND PATRICIA SCHMIDT ³

¹*Max Planck Institute for Gravitational Physics (Albert Einstein Institute), D-14467 Potsdam, Germany*

²*Instituto de Física Teórica UAM/CSIC, Universidad Autónoma de Madrid, Cantoblanco 28049 Madrid, Spain*

³*School of Physics and Astronomy and Institute for Gravitational Wave Astronomy, University of Birmingham, Edgbaston, Birmingham, B15 2TT, United Kingdom*

ABSTRACT

We revisit the population properties of neutron star-black hole (NSBH) mergers using low-mass compact binary coalescences reported through GWTC-4. Employing PYEFPE, an inspiral-only waveform model that captures both orbital eccentricity and spin-induced precession, we reanalyse all binary neutron star (BNS) and NSBH events observed via gravitational waves. The BNS systems GW170817 and GW190425 are fully consistent with quasi-circular inspirals, while GW200105 stands out among the NSBH binaries as the only system exhibiting significant residual eccentricity at 20 Hz, strengthening evidence for dynamically driven formation pathways. The remaining NSBH events show no measurable eccentricity and appear broadly compatible with low-spin binaries formed through isolated stellar evolution. Using hierarchical Bayesian inference, we obtain the first joint constraints on the mass, spin, and eccentricity distributions of NSBH binaries. Our results also yield the first simultaneous constraints on spin precession and orbital eccentricity in NSBH mergers, while the inferred merger rates remain fully consistent with previous LVK measurements. Treating all NSBH systems as a single population yields results compatible with formation in hierarchical triples, whereas the quasi-circular population remains broadly consistent with isolated evolution. Our results highlight the emerging role of eccentricity as a key discriminator between formation channels. As the number of NSBH detections grows, joint constraints on masses, spins, and orbital eccentricity will enable increasingly sharp tests of dynamical versus isolated binary evolution, establishing NSBH systems as powerful probes of compact-object astrophysics.

1. INTRODUCTION

Gravitational-wave (GW) observations with the Laser Interferometer Gravitational-Wave Observatory (LIGO) (J. Aasi et al. 2015), Virgo (F. Acernese et al. 2015) and KAGRA (T. Akutsu et al. 2021) (LVK) are a unique window into astrophysical populations of compact objects, allowing us to characterize the underlying distributions of their masses, spins, eccentricities, and their redshift-dependent merger rates. These population properties encode the physics of stellar evolution, binary dynamics, and compact object formation. Identifying the binary formation channels is one of the largest open questions in modern astrophysics, with important consequences for stellar physics, binary evolution, and relativistic astrophysics.

The groundbreaking observation of the mergers between neutron stars and black holes (R. Abbott et al. 2021a) provided unambiguous evidence for the existence

of these systems, which has been strengthened by subsequent observations (R. Abbott et al. 2023a; A. G. Abac et al. 2024, 2025a). This has triggered a series of investigations into the astrophysical properties of neutron star-black hole (NSBH) mergers and neutron star physics (A. M. Farah et al. 2022; P. Landry & J. S. Read 2021; C. Ye & M. Fishbach 2022; J.-P. Zhu et al. 2022; S. Biscoveanu et al. 2022b). It is of particular interest to disentangle the different scenarios for the evolutionary pathways of NSBH mergers.

Although numerous models have been proposed, see F. S. Broekgaarden et al. (2021) and references therein, the exact astrophysical processes at work remain highly uncertain. In the currently favored canonical scenario, NSBH systems form through isolated evolution of massive binaries undergoing a common envelope phase (K. Belczynski et al. 2001; M. Mapelli & N. Giacobbo 2018; P. Drozda et al. 2022; F. S. Broekgaarden et al. 2021; F. S. Broekgaarden & E. Berger 2021; I. Mandel & R. J. E. Smith 2021; Z. Xing et al. 2024). This scenario leads to several core predictions for the astro-

physical properties of these binaries. For example, natal black holes may be born with low spins if angular momentum transport between the helium core and hydrogen envelope, combined with envelope stripping, efficiently removes angular momentum from the progenitor (Y. Qin et al. 2018; J. Fuller & L. Ma 2019). While black holes are expected to form at wide orbits, tidal interactions in close binaries can potentially induce significant spin (E. Van den Heuvel & S.-C. Yoon 2007; D. Kushnir et al. 2016; Y. Qin et al. 2018; I. Mandel & T. Fragos 2020). The resulting spins are expected to be approximately aligned with the orbital angular momentum due to tidal interactions, though supernova kicks can induce misalignment (V. Kalogera 2000; D. Wysocki et al. 2018; N. Giacobbo & M. Mapelli 2019; M. Oh et al. 2023). These binaries should have negligible orbital eccentricity by the time they enter the LIGO-Virgo-KAGRA (LVK) sensitivity band, as eccentricity is very efficiently radiated away P. C. Peters (1964). However, it is important to note that mechanisms such as mass transfer (K. A. Rocha et al. 2025; Y. Zenati et al. 2025) and supernova kicks (N. Brandt & P. Podsiadlowski 1995; V. Kalogera 1996; A. Vigna-Gómez 2025) can challenge the assumption that residual eccentricity must always be negligible in isolated binary evolution.

In contrast, evolutionary pathways that involve dynamical interactions can lead to markedly different predictions for the properties of NSBH binaries. A wide range of such dynamical channels have been proposed. First, NSBH systems may form through dynamical assembly in dense stellar environments, including globular clusters (S. F. Portegies Zwart & S. McMillan 2000; P. C. C. Freire et al. 2004; C. S. Ye et al. 2019; M. Zevin et al. 2019; M. A. Sedda 2020; G. Fragione & S. Banerjee 2020; A. Dorozzmai et al. 2025) and young stellar clusters (S. F. Portegies Zwart & S. McMillan 2000; S. Rastello et al. 2020; A. A. Trani et al. 2022), where repeated few-body encounters can assemble compact binaries or form hierarchical triples through dynamical interactions. In globular clusters, however, the NSBH merger rate is expected to be highly suppressed. Ultra-wide binaries may be driven to merger through secular torques from the Galactic potential (E. Michaely & S. Naoz 2022; J. Stegmann et al. 2024), though the resulting rates depend sensitively on assumptions about natal kicks (E. Michaely & S. Naoz 2022). Additional dynamical mechanisms include fly-by interactions and direct gravitational-wave captures (B.-M. Hoang et al. 2020), although these channels generally predict comparatively low merger rates. Active galactic nuclei offer another pathway, in which gas torques and migration traps can efficiently drive compact binaries toward coalescence (N. C. Stone et al.

2017; Y. Yang et al. 2020; B. McKernan et al. 2020), but these predictions come with substantial astrophysical uncertainties. Finally, NSBH mergers can arise in hierarchical multiple systems, particularly stellar triples (K. Silsbee & S. Tremaine 2017; F. Antonini et al. 2017; A. S. Hamers & T. A. Thompson 2019; G. Fragione & A. Loeb 2019; A. A. Trani et al. 2022; J. Stegmann & J. Klencki 2025), some of which naturally form in young clusters (hence the dual appearance of A. A. Trani et al. 2022). In such systems, a bound tertiary companion induces secular gravitational perturbations through the von Zeipel–Kozai–Lidov (ZKL) mechanism (H. von Zeipel 1910; M. L. Lidov 1962; Y. Kozai 1962), generating large-amplitude eccentricity oscillations that can both accelerate the inspiral and significantly enhance the merger rate, while imprinting distinctive signatures such as residual eccentricity and spin–orbit misalignment. This final class is particularly appealing given the observational support that most massive progenitor stars are in hierarchical triples (M. Moe & R. Di Stefano 2017).

A key feature of dynamical formation channels is that they can naturally predict substantial spin-orbit misalignment and, in many cases, non-negligible residual orbital eccentricity even at relatively high gravitational-wave frequencies. The recent observation of measurable eccentricity in GW200105 (G. Morras et al. 2025a), one of the NSBH binaries reported by the LVK, is therefore difficult to reconcile with expectations from isolated binary evolution. Any eccentricity observed in the detector band must have been even larger at earlier times due to the rapid circularization driven by gravitational-wave emission (P. C. Peters 1964). This strengthens the case for exploring alternative, dynamically driven formation scenarios.

Recent work has strengthened this tension. In particular, J. Stegmann & J. Klencki (2025) show that the combination of residual eccentricity, spin-orbit misalignment, and the inferred NSBH merger rate is naturally explained if a significant fraction of NSBH mergers originate from hierarchical triple systems. The three-body dynamics of compact unequal-mass triples drives mergers across a broad range of orbital parameters whilst avoiding finely tuned tertiary inclinations. Such systems can retain measurable eccentricity down to gravitational-wave frequencies, providing a compelling formation pathway for events like GW200105.

Simultaneously, tentative hints for eccentricity are emerging in the binary black hole (BBH) population (I. M. Romero-Shaw et al. 2022; N. Gupte et al. 2025; M. d. L. Planas et al. 2025b; Y. Xu et al. 2025), though recent analyses also suggest that the branching ratio for eccentric events is below 0.0239 at 90% confi-

dence (M. Zeeshan et al. 2026), with the rate of eccentric binaries being only weakly constrained by observations and remaining highly model-dependent.

Motivated by these developments, we revisit the population properties of NSBH binaries using gravitational-wave data alone. In particular, we reanalyse all low-mass events observed to date to assess whether current observations already favour a multi-channel formation picture or remain consistent with a predominantly isolated binary origin. We perform a joint analysis of the mass, spin, and eccentricity distributions, as this remains one of the most powerful ways to discriminate between the plethora of formation channels for compact binaries (T. A. Callister 2024; J. Stegmann et al. 2025b; J. Stegmann & J. Klencki 2025). An advantage to our analysis is that we use a recently developed waveform model, PYEFPE (G. Morras et al. 2025b), that allows us to jointly infer spin-precession and orbital eccentricity. Due to the extremely limited number of BNS observations to date, we only report individual parameter estimation results for these binaries and do not attempt to model the astrophysical population.

2. ANALYSIS METHODS

In this section, we describe the methodology used to analyze the GW events. This includes the parameter estimation framework, the waveform models employed, the selection criteria for the events included in this study, and the specific configuration used for their analyses.

2.1. Parameter Estimation Framework

We perform coherent Bayesian parameter estimation to infer the source properties of each GW event. Parameter inference is carried out using nested sampling (J. Skilling 2006), as implemented in DYNesty (J. S. Speagle 2020a) within the BILBY inference framework (G. Ashton et al. 2019a). This allows us to sample the posterior distribution

$$p(\boldsymbol{\lambda} | d) = \frac{\mathcal{L}(d | \boldsymbol{\lambda}) \pi(\boldsymbol{\lambda})}{\mathcal{Z}(d)}, \quad (1)$$

where $\mathcal{L}(d | \boldsymbol{\lambda})$ is the likelihood of observing the data d given source parameters $\boldsymbol{\lambda}$, $\pi(\boldsymbol{\lambda})$ the prior, and $\mathcal{Z}(d)$ the Bayesian evidence.

Assuming stationary Gaussian noise in each detector, the likelihood of observing a GW signal $h(\boldsymbol{\lambda})$ in a network of N detectors is (J. Veitch et al. 2015)

$$\mathcal{L}(d | \boldsymbol{\lambda}) \propto \exp \left[-\frac{1}{2} \sum_{i=1}^N \langle h_i(\boldsymbol{\lambda}) - d_i | h_i(\boldsymbol{\lambda}) - d_i \rangle \right], \quad (2)$$

where $h_i(\boldsymbol{\lambda})$ denotes the predicted gravitational wave signal in the i -th detector and d_i the corresponding

strain data. The noise-weighted inner product $\langle \cdot | \cdot \rangle$ is defined as

$$\langle a | b \rangle = 4 \Re \int_{f_{\text{low}}}^{f_{\text{high}}} \frac{\tilde{a}(f) \tilde{b}^*(f)}{S_n(f)} df, \quad (3)$$

with $\tilde{a}(f)$ and $\tilde{b}(f)$ denoting the Fourier transforms of the time-domain functions $a(t)$ and $b(t)$, and $S_n(f)$ the one-sided power spectral density of the detector noise. The integration is performed over the frequency interval $[f_{\text{low}}, f_{\text{high}}]$.

2.2. Waveform Models

As described in Sec. 2.1, Bayesian parameter estimation requires predictions of the GW signal $h(\boldsymbol{\lambda})$ as a function of the source parameters $\boldsymbol{\lambda}$. Since a single analysis involves evaluating the likelihood tens of millions of times, it is essential to employ waveform models that are not only accurate but also computationally efficient. However, the general relativistic two-body problem is very complex and rich in physical effects, and even the most advanced waveform models make approximations to remain tractable. Models that are fast enough for large-scale inference often neglect key features such as orbital eccentricity, spin-induced precession, higher-order harmonics, or the merger-ringdown phase. To capture the relevant physics across different scenarios, we use three different waveform models:

- PYEFPE (G. Morras et al. 2025b): A frequency-domain, post-Newtonian (PN) model for inspiralling precessing-eccentric compact binaries. This waveform omits the merger-ringdown phase and is valid only for frequencies below the innermost stable circular orbit (ISCO). It models the GW amplitudes at Newtonian-order, corresponding to only having the $(l, |m|) = (2, 2)$ and $(2, 0)$ modes for eccentric binaries. The model incorporates eccentric harmonics through closed-form Fourier-Bessel amplitudes.
- IMRPHENOMXP (G. Pratten et al. 2021): A frequency-domain model for the full inspiral-merger-ringdown of precessing, quasi-circular binaries. The inspiral is based on the PN formalism, while the merger and ringdown are described using a phenomenological ansatz. This waveform is calibrated against effective-one-body and numerical relativity simulations. In the co-precessing frame (P. Schmidt et al. 2011), IMRPHENOMXP includes only the leading $(l, |m|) = (2, 2)$ mode (G. Pratten et al. 2020a).
- IMRPHENOMXPHM (G. Pratten et al. 2021): An extension of IMRPHENOMXP that includes higher-

order modes (HMs) (C. García-Quirós et al. 2020). Specifically, in the co-precessing frame it includes the $(l, |m|) = (2, 2), (2, 1), (3, 3), (3, 2),$ and $(4, 4)$ modes.

We note that all models used in this work describe binary black holes. In particular, they neglect tidal deformability and other matter effects that could be relevant if one or both components were neutron stars.

2.3. Event Selection

In this work, we study orbital eccentricity and spin-induced precession in a subset of GW events observed by the LVK detector network. We focus on low-mass binary coalescences, where at least one component is consistent with a NS, as their signals are dominated by the inspiral phase, where these effects are both most detectable and can be accurately modeled using PYEFPE. For such systems, the merger and ringdown occur at high frequencies, beyond the most sensitive band of current ground-based detectors, making them particularly well-suited for analysis with inspiral-only waveform models.

We restrict our analyses to events reported up to the GWTC-4 catalog (B. P. Abbott et al. 2019a; R. Abbott et al. 2021b, 2024, 2023a; A. G. Abac et al. 2025a), which includes detections up to the first part of the fourth LVK observing run (O4a) and represents the most recent publicly available dataset at the time of writing. Based on these considerations, we include in our study the two binary neutron star (BNS) mergers GW170817 (B. P. Abbott et al. 2017) and GW190425 (B. P. Abbott et al. 2020), as well as five neutron star–black hole (NSBH) mergers: GW190426.152155, GW190917.114630 (R. Abbott et al. 2024), GW200105.162426, GW200115.042309 (R. Abbott et al. 2021a), and GW230529.181500 (A. G. Abac et al. 2024). For brevity, we omit the timestamps after the underscores when referring to these events throughout the rest of the text.

The selected events span total masses between $\approx 2.7 M_\odot$ for GW170817 (B. P. Abbott et al. 2019b) and $\approx 12 M_\odot$ for GW190917 (R. Abbott et al. 2024). Their signal-to-noise ratios (SNRs) range from ≈ 9.5 for GW190917 (R. Abbott et al. 2024) to ≈ 32.4 for GW170817 (B. P. Abbott et al. 2017).

We exclude some of the LVK-reported events with component masses consistent with containing at least one neutron star. In particular, GW191219.163120 and GW200210.092254 (R. Abbott et al. 2023a) are excluded due to their significantly higher total masses ($\approx 32 M_\odot$ and $\approx 27 M_\odot$, respectively) and moderate SNRs (≈ 8.9 and ≈ 9.5 respectively), which limits the applicability of inspiral-only models. GW230518.125908 (A. G. Abac

et al. 2025a) is excluded because it was identified during the engineering run preceding O4a. Finally, we exclude GW190814 (R. Abbott et al. 2020), which has a $2.59_{-0.09}^{+0.08} M_\odot$ secondary, slightly above the expected maximum neutron star mass (L. Rezzolla et al. 2018; B. Margalit & B. D. Metzger 2017; M. Shibata et al. 2019; Y.-Z. Fan et al. 2024). Despite its relatively high total mass ($\approx 26 M_\odot$), the event has a large total SNR (≈ 25), with a substantial amount of it accumulated during the inspiral. However, we do not include it in our analysis, as the strong contribution of higher-order modes, absent in PYEFPE, could bias the inferred parameters.

2.4. Data Selection and Analysis Settings

We analyze the selected events using publicly available strain data, noise power spectral densities, and calibration envelopes (LIGO-Virgo Collaboration 2017; R. Abbott et al. 2021c, 2023b; LVK Collaboration 2020a,b,c; LVK Collaboration 2022, 2021, 2023a,b; A. G. Abac et al. 2024). For events affected by known noise transients, we use the corresponding BayesWave-deglitched strain data (N. J. Cornish & T. B. Littenberg 2015; N. J. Cornish et al. 2021). In particular, GW170817 was affected by a prominent blip glitch in the LIGO-Livingston detector less than 1 s before merger. GW190425 had a short glitch in LIGO-Livingston about 60 s before merger. GW200105 exhibited minor scattered light noise artifacts in LIGO-Livingston below 25 Hz, occurring approximately 3 s before merger. Finally, GW200115 was affected by more pronounced scattered light noise in LIGO-Livingston below 25 Hz.

We set the low-frequency cut-off to $f_{\text{low}} = 20$ Hz for all events except for GW170817. For this event, we use a slightly higher value of $f_{\text{low}} = 23$ Hz, both because it was observed during the second observing run (O2), when low-frequency sensitivity was significantly worse than in O3 and O4 (A. Buikema et al. 2020; E. Capote et al. 2025), and to limit the waveform duration to less than 128 s to reduce the computational cost consistent with the analyses presented by the LVK (B. P. Abbott et al. 2019a).

The high-frequency cut-off, f_{high} , is conservatively set below the frequency of the minimum energy circular orbit (MECO) (M. Cabero et al. 2017; G. Pratten et al. 2021) obtained from the posterior samples from publicly available analyses. This choice ensures that the analysis remains within the regime of validity of the PN approximations used in PYEFPE. The value of f_{high} used for each event is listed in Table 1. For NSBH events, f_{high} is chosen just below f_{MECO} , while for BNS systems (GW170817 and GW190425), we adopt an even more conservative value of $f_{\text{high}} = 400$ Hz, well below

Event	f_{high} [Hz]	$\mathcal{M}_c^{\text{det}}$ [M_{\odot}]	Duration [s]
GW170817	400	[1.195, 1.200]	128
GW190425	400	[1.475, 1.495]	128
GW190426	350	[2.4, 2.8]	64
GW190917	190	[3.6, 4.6]	32
GW200105	340	[3.45, 3.70]	32
GW200115	370	[2.4, 2.8]	64
GW230529	566	[2.01, 2.04]	128

Table 1. High-frequency cut-off (f_{high}) in Hz, detector-frame chirp mass ($\mathcal{M}_c^{\text{det}}$) prior range in solar masses (M_{\odot}), and segment duration in seconds (s) used in the parameter estimation analyses for each event.

f_{MECO} , to avoid the high-frequency regime where tidal effects, absent in the waveform models employed, can play a significant role in nearly equal-mass systems (E. E. Flanagan & T. Hinderer 2008; I. Harry & T. Hinderer 2018; G. Pratten et al. 2022).

We adopt broad, uninformative priors in the parameter estimation analyses. These priors are designed to cover the entire region of parameter space where the likelihood has significant support, helping avoiding biases in parameter recovery and ensuring the posteriors are suitable for reweighting in population analyses. Specifically, we use priors that are uniform in the detector-frame component masses and dimensionless spin magnitudes $\chi_1, \chi_2 \in [0, 0.8]$, isotropic in spin orientations, binary inclination, and sky position, and uniform in comoving volume and source-frame coalescence time. The component mass priors are constrained to ensure a mass ratio $q = m_2/m_1 \in [0.05, 1]$ and a detector-frame chirp-mass that spans the range listed in Table 1. For analyses including orbital eccentricity, we adopt a uniform prior on the eccentricity $e_{20\text{Hz}} \in [0, 0.4]$, defined at a reference GW frequency of 20 Hz, and a uniform prior on the mean anomaly.

The duration of the data segment analyzed for each event, also shown in Table 1, is chosen to fully contain the longest possible signal given the prior bounds and frequency range.

3. RESULTS

In this section, we present the results of the single-event eccentric-precessing parameter estimation analyses, separating the discussion of the BNS and NSBH systems. We report the following parameters: the source-frame component masses m_i^{source} , the eccentricity $e_{20\text{Hz}}$ defined at a GW reference frequency of 20 Hz, the luminosity distance D_L in Mpc, and the two effective spin parameters that capture the dominant spin-orbit contributions to the gravitational-wave signal. The first effective parameter is the mass-weighted projection of the component spins

along the direction of the Newtonian orbital angular momentum, \hat{L}_N (T. Damour 2001; E. Racine 2008; P. Ajith et al. 2011),

$$\chi_{\text{eff}} = \left(\frac{m_1}{M} \chi_1 + \frac{m_2}{M} \chi_2 \right) \cdot \hat{L}_N, \quad (4)$$

where $M = m_1 + m_2$ and $\chi_i = \mathbf{S}_i/m_i^2$. The second is an effective precession parameter defined at the reference frequency, which quantifies the degree of relativistic precession induced by spin-orbit misalignment (P. Schmidt et al. 2015),

$$\chi_p = \max \left[\chi_1 \sin \theta_1, \left(\frac{3+4q}{4+3q} \right) q \chi_2 \sin \theta_2 \right], \quad (5)$$

where $q = m_2/m_1 \leq 1$ and θ_i denotes the tilt angle between χ_i and \hat{L}_N .

3.1. Binary Neutron Stars

The marginal posterior distributions for selected source parameters of the BNS events are shown in Fig. 1. Due to their long inspiral durations in band, the parameters of these systems are tightly constrained, particularly for GW170817, which was observed with an SNR of approximately 32 (B. P. Abbott et al. 2017). We find that both BNS events are consistent with a quasi-circular inspiral. At the 90% credible level, we constrain the eccentricities at 20 Hz to $e_{20\text{Hz}}^{\text{GW170817}} < 0.011$ and $e_{20\text{Hz}}^{\text{GW190425}} < 0.022$, respectively. We report eccentricity constraints at 20 Hz because this is the frequency from which the data are analyzed, thereby avoiding extrapolation to unobserved frequencies.

Nonetheless, for comparison with the literature, we can convert these constraints to a reference frequency of 10 Hz using that (P. C. Peters 1964)

$$\frac{f_1}{f_2} = \left(\frac{e_2}{e_1} \right)^{18/19} \left(\frac{1-e_2^2}{1-e_1^2} \right)^{-3/2} \left(\frac{1 + \frac{121}{304} e_2^2}{1 + \frac{121}{304} e_1^2} \right)^{1305/2299}, \quad (6)$$

where e_1 and e_2 correspond to the eccentricities measured at frequencies f_1 and f_2 , respectively. Using this relation, the 90% credible upper limits translate to $e_{10\text{Hz}}^{\text{GW170817}} < 0.022$ and $e_{10\text{Hz}}^{\text{GW190425}} < 0.046$, in agreement with previous constraints reported in A. K. Lenon et al. (2020).

Consistent with the lack of evidence for eccentricity, Fig. 1 shows that the parameters estimated with PYEFPE are in good agreement with those obtained using the IMRPHENOMXP and IMRPHENOMXPHM approximants. In particular, GW170817 has component masses compatible with neutron stars observed in Galactic binary systems (T. M. Tauris et al. 2017), and spins that are consistent with being small. In contrast, GW190425 favors larger component masses which,

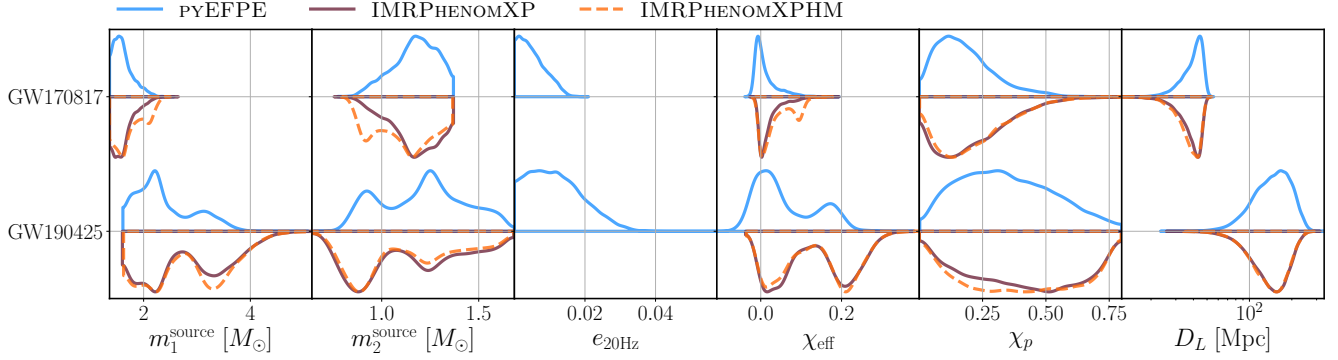


Figure 1. Marginal posterior distributions for selected source parameters of the two BNS events. Shown are the source-frame component masses (m_1^{source} and m_2^{source}), eccentricity at 20Hz ($e_{20\text{Hz}}$), the effective inspiral spin (χ_{eff}), the effective precession spin (χ_p), and the luminosity distance (D_L). In each violin plot, the upper half corresponds to results from the eccentric pYEFPE analysis, while the lower half shows posteriors from the quasi-circular IMRPHENOMXP (solid) and IMRPHENOMXPHM (dashed) analyses.

while still compatible with neutron stars, are not representative of the observed Galactic binary neutron star population (P. Landry & J. S. Read 2021). Moreover, due to its significantly lower SNR, the spin parameters are only weakly constrained.

3.2. Neutron Star - Black Holes

The marginal posterior distributions for selected source parameters of the NSBH events are shown in Fig. 2. Among these, GW200105 stands out as a clear outlier, being the only event whose eccentricity posterior peaks significantly away from zero. This behavior has been studied in detail in (G. Morras et al. 2025a; M. d. L. Planas et al. 2025a; A. Jan et al. 2026; K. Kacanjanja et al. 2025; A. Tiwari et al. 2025). Notably, GW200105 also exhibits much narrower posteriors compared to the other NSBH events, likely due to the measurement of multiple orbital harmonics (G. Morras et al. 2025b).

The remaining events are consistent with being quasi-circular. In particular, the eccentricity posteriors of GW200115 and GW230529 are in good agreement with those reported in M. d. L. Planas et al. (2025a) and K. Kacanjanja et al. (2025), while, to our knowledge, no previous eccentric analyses have been performed for GW190426 and GW190917.

Excluding GW200105, whose inferred parameters are significantly modified by the presence of eccentricity, the remaining events in Fig. 2 show broad agreement between the parameters estimated with pYEFPE and those obtained using the quasi-circular IMRPHENOMXP and IMRPHENOMXPHM models. In general, these systems are consistent with being non-spinning, with primary masses that are relatively low compared to the black holes observed in binary black hole mergers (A. G. Abac et al. 2025b), and secondary masses that span the

full $\sim 1\text{--}2.3 M_\odot$ range where neutron stars are expected to reside (B. Kiziltan et al. 2013; P. Landry & J. S. Read 2021).

4. ASTROPHYSICAL IMPLICATIONS

4.1. Methodology

We characterize the population properties of astrophysical NSBH systems using individual event source parameters inferred with the pYEFPE model, employing hierarchical Bayesian inference following (I. Mandel et al. 2019; E. Thrane & C. Talbot 2019; R. Abbott et al. 2023c; S. Biscoveanu et al. 2022b; T. A. Callister 2024).

Given data $\{d\}$ consisting of N_{det} detected GW events, we infer the posterior on hyperparameters Λ characterizing the astrophysical population,

$$p(\Lambda|\{d\}) = \frac{\mathcal{L}(\{d\}|\Lambda)\pi(\Lambda)}{\mathcal{Z}_\Lambda}, \quad (7)$$

where $\pi(\Lambda)$ and \mathcal{Z}_Λ are the hyperparameter prior and evidence, respectively. Modeling the detected events as an inhomogeneous Poisson process (I. Mandel et al. 2019), the likelihood takes the form

$$\mathcal{L}(\{d\}, N_{\text{det}}|\Lambda) \propto N(\Lambda)^{N_{\text{det}}} e^{-N_{\text{exp}}(\Lambda)} \times \prod_{i=1}^{N_{\text{det}}} \int d\theta \mathcal{L}(d_i|\theta)\pi(\theta|\Lambda), \quad (8)$$

where $N(\Lambda)$ is the expected total number of mergers (detected and undetected) during the observing period, and

$$N_{\text{exp}}(\Lambda) = N(\Lambda)\alpha(\Lambda) \quad (9)$$

is the expected number of detections. The detectability fraction $\alpha(\Lambda)$ accounts for selection effects by giving the

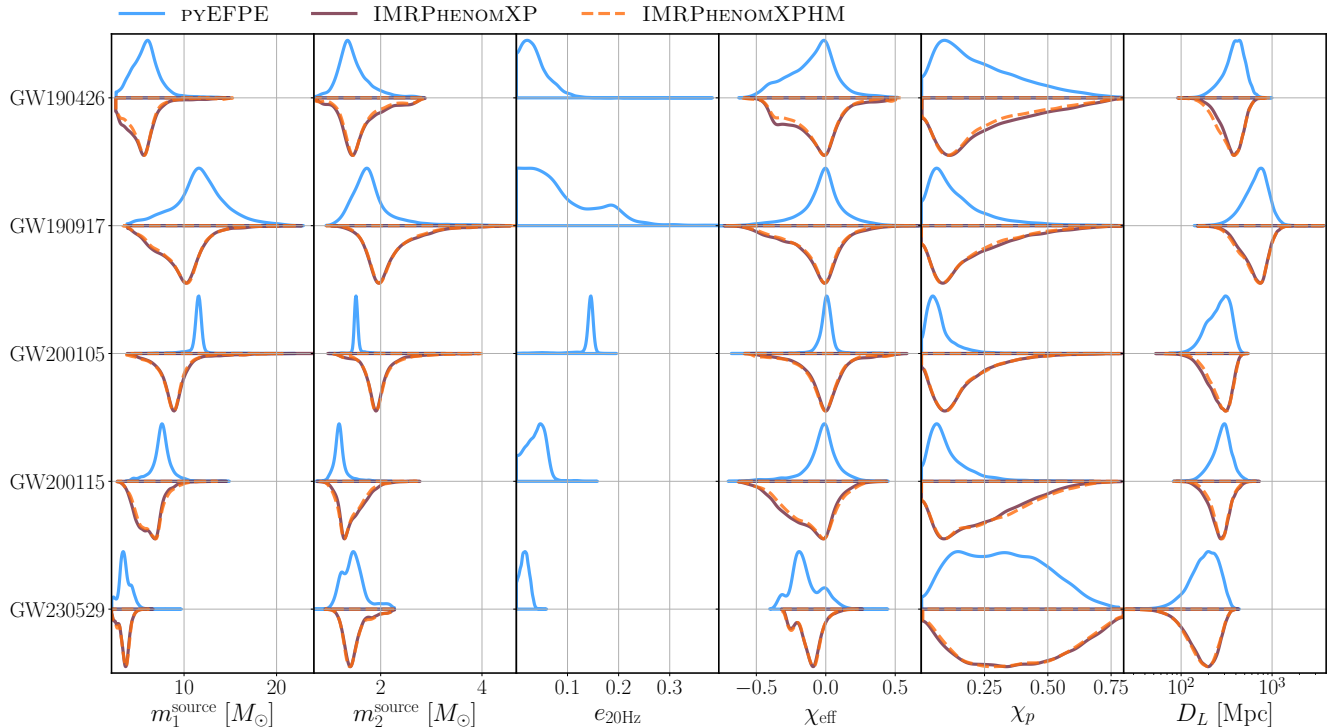


Figure 2. Marginal posterior distributions for selected source parameters of the selected NSBH events. Shown are the source-frame component masses (m_1^{source} and m_2^{source}), eccentricity at 20Hz ($e_{20\text{Hz}}$), the effective inspiral spin (χ_{eff}), the effective precession spin (χ_p), and the luminosity distance (D_L). In each violin plot, the upper half corresponds to results from the eccentric PYEFPE analysis, while the lower half shows posteriors from the quasi-circular IMRPHENOMXP (solid) and IMRPHENOMXPHM (dashed) analyses.

fraction of binaries drawn from the population model that would be detectable (T. J. Loredo 2004; I. Mandel et al. 2019). For each event i , $\mathcal{L}(d_i | \theta)$ is the likelihood of the strain data given source parameters θ , and $\pi(\theta | \Lambda)$ is the distribution of source parameters conditioned on the population hyperparameters Λ .

We compute $\alpha(\Lambda)$ via Monte Carlo integration following (W. M. Farr 2019), using sensitivity estimates for NSBH binaries derived from injection campaigns conducted in support of the LVK analyses (R. Abbott et al. 2021d; R. Essick 2026). We note that these selection effects do not yet account for orbital eccentricity, which we defer to future work; see (A. H. Nitz & Y.-F. Wang 2021; R. Dhurkunde & A. H. Nitz 2025; K. S. Phukon et al. 2025b,a) for progress on incorporating eccentricity into searches, and (M. K. Singh et al. 2025; I. Romero-Shaw et al. 2025) for efforts toward characterizing the observability of eccentricity in compact binary populations.

Our exploration of the NSBH population is largely templated on the analysis by S. Biscoveanu et al. (2022b). Here we outline the specific choices made in our analysis. We model the black hole mass distribution as a truncated

power-law, such that

$$\pi(m_{\text{BH}} | \alpha, m_{\text{BH},\text{min}}, m_{\text{BH},\text{max}}) \propto \begin{cases} m_{\text{BH}}^{-\alpha}, & m_{\text{BH},\text{min}} \leq m_{\text{BH}} \leq m_{\text{BH},\text{max}} \\ 0, & \text{otherwise} \end{cases} \quad (10)$$

For the mass ratio, we use the truncated Gaussian model proposed in (M. Fishbach & D. E. Holz 2020; S. Biscoveanu et al. 2022b)

$$\pi(q | m_{\text{BH}}, m_{\text{NS},\text{max}}, \mu, \sigma) \propto \begin{cases} \mathcal{N}(q | \mu, \sigma), & q_{\text{min}}(m_{\text{BH}}) \leq q \leq q_{\text{max}}(m_{\text{BH}}, m_{\text{NS},\text{max}}) \\ 0, & \text{otherwise} \end{cases} \quad (11)$$

which describes the conditional pairing distribution between black holes and the neutron stars. As in (S. Biscoveanu et al. 2022b), we assume that the black hole is always the more massive of the two compact objects in the binary with the minimum neutron star mass taken to be $1M_{\odot}$ such that $q_{\text{min}} = 1/m_{\text{BH},\text{max}}$. The maximum neutron star mass is taken as a free hyperparameter to be constrained by the data.

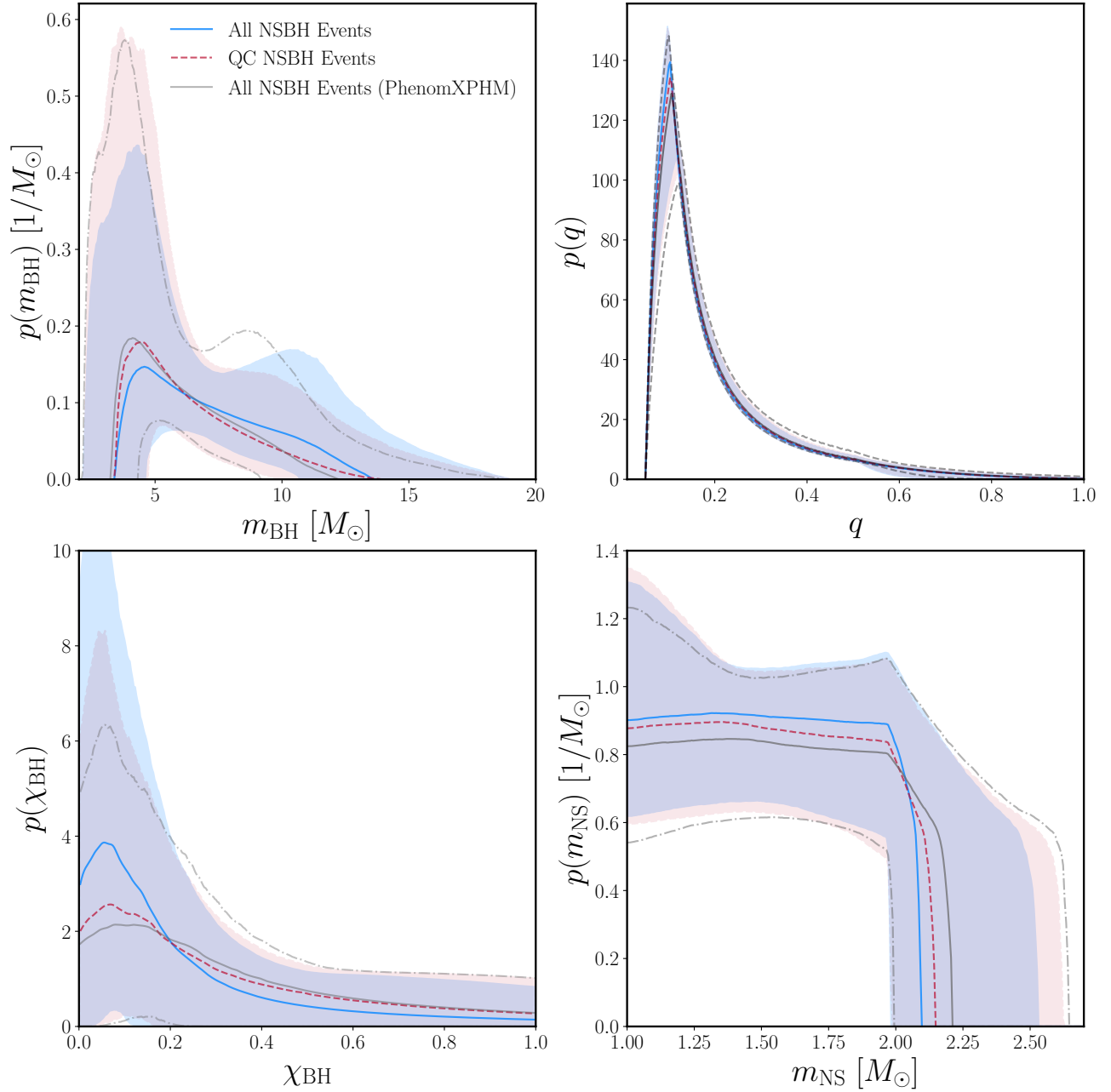


Figure 3. The median and 90% credible intervals of the population predictive distributions for the black hole mass, the mass ratio, the black hole spin, and the neutron star mass. The blue curves analyses all NSBH events using pyEFPE, the red curve only the quasi-circular NSBH events, and the grey curve all NSBH events but using IMRPhenomXPHM (i.e. neglecting eccentricity).

Following (A. G. Abac et al. 2025b), the black hole spin magnitude is taken to follow a truncated Normal distribution parameterized by $\{\mu_\chi, \sigma_\chi\}$,

$$\pi(\chi_{\text{BH}}|\mu_\chi, \sigma_\chi) = \mathcal{N}_{[0,1]}(\chi_{\text{BH}}|\mu_\chi, \sigma_\chi). \quad (12)$$

We adopt the truncated Normal distribution over the Beta distributions, see (D. Wysocki et al. 2019), as these are known to enforce $p(\chi) = 0$ at $\chi = 0$ and $\chi = 1$,

failing to model contributions to the population at near-zero and near-extremal spins respectively (A. G. Abac et al. 2025b). The black hole spin orientation, denoted by $z_{\text{BH}} = \cos\theta_{\text{BH}}$, is modeled as an admixture of two populations (C. Talbot & E. Thrane 2017): a population with spins preferentially aligned with the orbital angular momentum and a population with isotropically oriented spins. These are intended to broadly capture contribu-

tions from the isolated evolution channel and contributions from dynamical formation scenarios. Adopting the model proposed in (S. Vitale et al. 2022), the preferentially aligned population is described by a truncated Gaussian in z_{BH} with mean μ_t and standard deviation σ_t , such that

$$\pi(z_{\text{BH}} | \xi, \mu_t, \sigma_t) = (1 - \xi) \frac{1}{2} + \xi \mathcal{N}_{[-1,1]}(z_{\text{BH}} | \mu_t, \sigma_t). \quad (13)$$

Here, ξ denotes the fraction of binaries in the preferentially aligned population. We do not model the neutron star spin distribution, as we expect this to remain largely unresolved given current detector sensitivities. Instead, following (S. Biscoveanu et al. 2022b), we adopt a physical constraint that the neutron star spins remains below the mass-shedding limit of $\chi_{\text{Kep}} \sim 0.7$ (D.-S. Shao et al. 2020; E. R. Most et al. 2020).

For the eccentricity, in lieu of a more astrophysically motivated model, we explore two different population models. The first model, adopted as our default model, introduces a truncated normal to bound the mean and variance of the eccentricity in the population

$$\pi(e | \mu_e, \sigma_e) \propto \begin{cases} \mathcal{N}(e | \mu_e, \sigma_e), & 0 \leq e \leq 1 \\ 0, & \text{otherwise} \end{cases}. \quad (14)$$

We emphasize that the eccentricity distribution adopted here is a phenomenological parametrization rather than an astrophysically motivated model. Given the paucity of confidently measured eccentric binaries, the aim is to quantify how far from zero the population is allowed to deviate, without imposing any specific physical form on the underlying distribution.

A related model is the generalization to an admixture model designed to capture contributions from low-eccentricity (isolated evolution) and high-eccentricity (dynamical) formation channels,

$$\pi(e | \lambda_{\text{qc}}, \mu_{\text{dyn}}, \sigma_{\text{qc}}, \sigma_{\text{dyn}}) = \lambda_{\text{qc}} \mathcal{N}_{[0,1]}(e | 0, \sigma_{\text{qc}}) + (1 - \lambda_{\text{qc}}) \mathcal{N}_{[0,1]}(e | \mu_{\text{dyn}}, \sigma_{\text{dyn}}). \quad (15)$$

The quasi-circular population is parameterized by $\{\mu_{\text{qc}} = 0, \sigma_{\text{qc}}\}$, and the dynamical population by $\{\mu_{\text{dyn}}, \sigma_{\text{dyn}}\}$. The fraction of binaries in the quasi-circular population is controlled by the hyperparameter λ_{qc} .

In practice, we use the GWPOPULATION package (C. Talbot et al. 2019) together with the nested sampler DYNESTY (J. S. Speagle 2020b), as implemented in BILBY (G. Ashton et al. 2019b), to draw posterior samples from the distribution $p(\Lambda | \{d\})$. We use uniform priors on all population hyperparameters, with the ranges

reported in Table 2. Population predictive distributions (PPD),

$$p(\theta | \{d\}) = \int \pi(\theta | \Lambda) p(\Lambda | \{d\}) d\Lambda, \quad (16)$$

are used to show the impact of assumptions on event selection on the anticipated astrophysical distribution of binary source parameters θ conditional on the observed events.

4.2. Population Properties

Before discussing the inferred astrophysical population properties, we emphasize that current NSBH population inferences rely on only a handful of confidently identified events. As a consequence, the inferred distributions of masses, spins, and eccentricities remain sensitive to individual systems, and population-level conclusions should be interpreted with appropriate caution. At the same time, the presence of even a single confidently measured eccentric NSBH merger highlights the potential importance of dynamical formation pathways and motivates comparison with theoretical predictions. As the number of NSBH detections grows, our ability to disentangle the contributions from multiple channels will improve substantially.

Fundamentally, we expect a broad range of astrophysical formation channels to contribute to the overall NSBH merger rate, each of which will predict a range of masses, spins, and eccentricities. With only a limited set of NSBH observations, we cannot meaningfully extract the branching ratios. To interpret the observed NSBH population, we therefore consider a few broad hypotheses. In the first, we assume that all NSBH mergers originate from a single underlying population and therefore analyse the entire sample together. Although the significant eccentricity of GW200105 rules out an origin through isolated binary evolution, the properties of the full observed NSBH sample remain consistent with expectations from hierarchical triple evolution. In particular, J. Stegmann & J. Klencki (2025) show that hierarchical triples can reproduce the observed NSBH merger rate and key population features, including large spin-orbit misalignment and residual eccentricity, with the probability of generating an event with $e_{20} \geq 0.145$, as inferred for GW200105 (G. Morras et al. 2025a), being approximately 25%. In this framework, all NSBH events observed to date, including the eccentric binary, can be explained without invoking additional formation channels. This allows us to treat the full catalogue as a single population in this scenario, while noting that a more detailed accounting of channel contributions will require more detections.

In the second hypothesis, we assume that the eccentric event GW200105 represents a distinct formation

pathway and therefore exclude it from the population analysis. The remaining NSBH mergers exhibit properties consistent with those expected from isolated binary evolution (F. S. Broekgaarden et al. 2021; F. S. Broekgaarden & E. Berger 2021). We refer to this subset as the quasi-circular (QC) population and use it to characterize the mass distribution, spin orientations, and expected residual eccentricities of NSBH binaries that plausibly arise from isolated evolution. The QC population is anticipated to exhibit low eccentricity, efficient tidal circularization, and preferential spin-orbit alignment due to the binary’s stable evolutionary history. By isolating this subset, we can assess whether the observed QC events are consistent with standard isolated formation channels, and explore the extent to which their inferred population properties differ from those obtained when all events are treated as part of a single, coherent NSBH population. Within this quasi-circular subset, we find no compelling deviations from the expectations of isolated binary evolution: the inferred eccentricities remain consistent with efficient tidal circularisation, the spins show no evidence for strong misalignment, and the overall source properties broadly match those predicted by standard field-binary formation models (F. S. Broekgaarden et al. 2021).

The final scenario we consider employs a mixture model for the eccentricity distribution, as given in Eq. 15. In this scenario, we model two distinct contributions to the NSBH population arising from low-eccentricity (isolated binary evolution) and high-eccentricity (dynamical) formation channels. Whilst the eccentricity distribution is modeled by two components, we do not attempt a channel-by-channel decomposition of the mass and spin distributions. This is a pragmatic choice, as the eccentricity of GW200105 provides a clear discriminating observable that motivates the two-component model. In contrast, the mass and spin distributions predicted by different formation channels are expected to be highly degenerate. Given the limited number of current NSBH detections, the data lack the statistical power to meaningfully separate channel contributions in these parameters, and we therefore characterize the mass and spin properties of the *total* NSBH population without distinguishing between formation channels.

Having outlined the population scenarios under consideration, we now explore the inferred population properties, beginning with the black hole mass distribution. Unless otherwise stated, our comparisons will be between the first two scenarios discussed above, with the third scenario only entering into our discussion on eccentricity. As GW230529 is the lowest-mass NSBH observed to date, including this event shifts the minimum black hole mass to lower values, finding $m_{\min}^{\text{BH}} = 3.57_{-1.38}^{+1.17} M_{\odot}$

for the total NSBH population and $3.58_{-1.38}^{+1.21} M_{\odot}$ for the QC population. This is consistent with the lower black hole mass inferred in the GW230529 discovery paper (A. G. Abac et al. 2024). For the upper black hole mass, whether or not we include GW200105 only leads to a relatively small impact on the overall population. In (G. Morras et al. 2025a), the mass of the black hole was reported to be $m_{\text{BH}} = 11.5_{-1.6}^{+0.6}$, driving a peak in the population predictive distribution just above $10M_{\odot}$. Including GW200105 leads to a slight excess in more massive black hole masses and a slightly tighter bound on the maximum black hole mass of $m_{\max}^{\text{BH}} = 13.66_{-3.20}^{+5.48} M_{\odot}$ compared to $m_{\max}^{\text{BH}} = 13.95_{-4.27}^{+5.29} M_{\odot}$ when excluding the event. The shift towards a heavier upper limit in the black hole mass distribution relative to (S. Biscoveanu et al. 2022b) can be partially attributed to the shift to higher primary masses when using PYEFPE, as seen in Fig. 2.

The mass-ratio distribution is strongly driven by the priors on the maximum and minimum component masses, as discussed in (S. Biscoveanu et al. 2022b). Whilst the black hole mass and spin distributions are comparatively well constrained, the prior-dependence in the mass-ratio impacts the neutron star mass distribution in a non-trivial way. Adopting the priors used in (S. Biscoveanu et al. 2022b), the black holes are allowed to span a range $m_{\text{BH}} \in [2, 20]M_{\odot}$ and neutron stars $m_{\text{NS}} \in [1, 2.7]M_{\odot}$, resulting in the mass-ratio prior clustering around $q \sim 0.1$. We only consider the Gaussian model, as even with the additional events considered here, little information is gained relative to the earlier analysis in (S. Biscoveanu et al. 2022b). We find constraints on the maximum NS mass to be $m_{\max}^{\text{NS}} = 2.10_{-0.12}^{+0.46}$ when including GW200105 and $m_{\max}^{\text{NS}} = 2.15_{-0.16}^{+0.47}$ when excluding the event. We caveat that this is the maximum NS mass as inferred from the NSBH population in isolation, and does not take into account the BNS observations, notably GW190425 which has support for NS masses up to $m_{\text{NS}}^{\text{max}} \approx 2.52M_{\odot}$ assuming a high-spin prior (B. P. Abbott et al. 2020).

The distribution of the black hole spin magnitudes was modeled using a truncated Gaussian rather than a Beta distribution, which can help capture contributions to the population near $\chi \approx 0$ (A. G. Abac et al. 2025b). Consistent with earlier analyses, we find that the BH spin magnitudes in NSBH are systematically smaller than those inferred from the binary black hole (BBH) population (A. G. Abac et al. 2025b). Recent updated analyses of GW200105, see (G. Morras et al. 2025a), favour small black hole spins, finding $\chi_{\text{BH}} = 0.06_{-0.05}^{+0.18}$ or, in terms of the effective spin parameters, $\chi_{\text{eff}} = 0.005_{-0.095}^{+0.071}$ and $\chi_p = 0.06_{-0.04}^{+0.13}$. Due to the extremely well-constrained low-spin measurement,

whether or not we include GW200105 in the population has a notable impact on the χ_{BH} distribution. Nevertheless, the population predictive distribution for the black-hole spin magnitudes continues to favour low χ_{BH} , consistent with the emerging picture that NSBH systems may host systematically lower spins than those observed in BBH mergers.

For the spin-tilt distribution, unlike the BBH observations (A. G. Abac et al. 2025b; J. Stegmann et al. 2025a), the current NSBH population is only weakly constrained. Interestingly, even after excluding the GW200105, the quasi-circular NSBH binaries exhibit a mild preference for $\cos\theta_{\text{BH}} < 0$, see the bottom panel of Fig. 4, indicating a tendency toward spin-orbit misalignment. Although this trend is not yet statistically significant, it is qualitatively consistent with expectations from dynamically influenced formation channels. However, there are several factors that must be taken into account. For low-SNR events with $\chi_{\text{eff}} \approx 0$, and poorly constrained χ_p , the likelihood provides limited information about spin orientations. As such, the event-level posteriors are largely shaped by the prior volume, and the hierarchical inference for these parameters remains prior-dominated. This is coupled with a known degeneracy between the masses and spins of the binary components (C. Cutler & E. E. Flanagan 1994; A. G. Abac et al. 2024), in which more comparable mass ratios correlate with a more negative χ_{eff} , though the inclusion of spin-precession can help break this degeneracy (A. Vecchio 2004; K. Chatziioannou et al. 2015; G. Pratten et al. 2020b). This effect can be partially seen in Fig. 2, where the posterior distributions for χ_{eff} show a tail that is mildly negatively skewed, see also the discussion in (A. G. Abac et al. 2024). As a result, the mild preference for negative $\cos\theta_{\text{BH}}$ at the population level could be interpreted as a consequence of these prior-driven and degeneracy-driven effects, rather than as evidence for astrophysical spin-orbit misalignment, warranting further study.

In the hierarchical triple analysis presented in J. Stegmann & J. Klencki (2025), tertiary-induced NSBH mergers were found to occur in a strongly non-adiabatic regime in which the ZKL timescale is much shorter than the relativistic spin-precession timescale, i.e., $\tau_{\text{ZKL}} \ll \tau_p$. In this limit, the black hole spin precesses about the total angular momentum \mathbf{J} of the system while maintaining an approximately constant tilt angle relative to \mathbf{J} , whereas the orbital angular momentum vector undergoes large-amplitude reorientation. This naturally leads to a $\cos\theta_{\text{BH}}$ distribution that is broad and approximately symmetric about zero, leading to a non-negligible fraction of mergers ($\sim 10\text{--}20\%$ in the triple-channel models) with retrograde spin configurations. This behaviour is

consistent with recent analyses of non-adiabatic spin dynamics, such as C. L. Rodriguez & F. Antonini (2018), who showed that when the spin-precession timescale exceeds the ZKL timescale, the spin remains effectively fixed while the orbital plane reorients, naturally producing broad spin-tilt distributions. The population predictive distributions in Fig. 4 are in broad agreement with these predictions.

By contrast, isolated binary evolution through a common-envelope phase is expected to produce a distribution sharply peaked near $\cos\theta_{\text{BH}} \simeq 1$, unless large natal kicks are invoked. In particular, (G. Fragione et al. 2021) argued that for common-envelope evolution to result in large spin-orbit tilts, one would need natal kicks $\gtrsim 150 \text{ km s}^{-1}$ and highly efficient common-envelope ejection, $\alpha_{\text{CE}} \gtrsim 3$. Whilst our results are fairly uninformative, there is a slight tension with the isolated evolution predictions due to the mild preference for $\cos\theta_{\text{BH}} < 0$, as discussed above.

Dynamical assembly in star clusters is also expected to produce broadly distributed, and in some cases nearly isotropic, spin-tilt orientations (e.g. C. L. Rodriguez et al. 2016; B.-M. Hoang et al. 2020), but the NSBH merger rate from clusters is expected to be orders of magnitude below the inferred rates (A. G. Abac et al. 2025b), making this channel an unlikely contributor to the observed population.

For the eccentricity distributions, GW200105 shifts the mean of the truncated Normal model toward larger eccentricities, generating an extended high-eccentricity tail in the posterior predictive distribution (PPD; bottom panel of Fig. 4). We note that the 90% credible intervals are sensitive to the lower prior bound on the variance of the truncated Normal, σ_e , leading to the apparent gap in the predictive distribution around $e_{20\text{Hz}} \sim 0.02$. After marginalizing over hyperparameter uncertainty, we place 90% upper limits on the population eccentricity at 20,Hz of $e_{20\text{Hz}} < 0.11^{+0.17} - 0.09$ for the full NSBH sample and $e_{20\text{Hz}} < 0.05^{+0.15} - 0.04$ for the quasi-circular (QC) subset. The quoted uncertainties correspond to the 90% credible interval of the posterior predictive distributions.

Figure 5 presents a subset of the hyperparameters from the mixture model described in Eq. 15. The upper panel shows the population mean eccentricity of the dynamical component, μ_{dyn} , which exhibits a mild peak near the value inferred eccentricity of GW200105 (G. Morras et al. 2025a). The lower panel displays the mixing fraction between the quasi-circular and dynamical channels, λ_{qc} . Although this parameter remains weakly constrained, the posterior disfavors a purely dynamical population, consistent with the conclusions from event-level parameter estimation. The variances of the truncated Normal

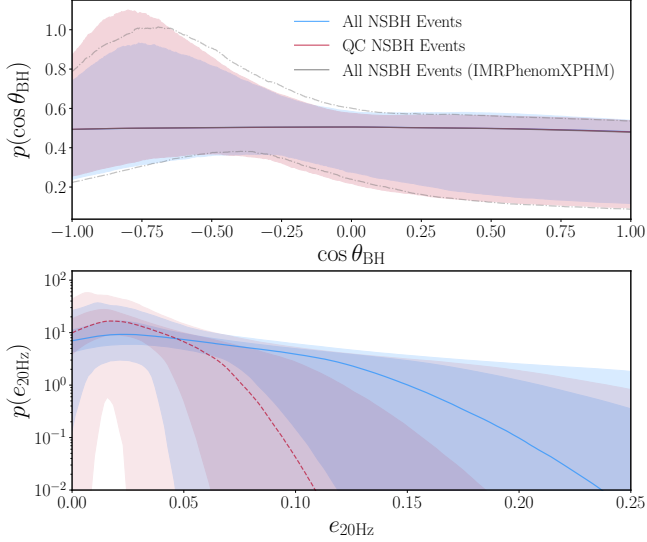


Figure 4. Population predictive distributions for the truncated Normal population model for eccentricity. The top panel shows the cosine of the black hole spin tilt angle $\cos\theta_{\text{BH}}$ and the lower panel the eccentricity at 20Hz.

components are likewise only weakly constrained, as expected given the limited number of observations. The remaining population hyperparameters are consistent with those obtained under the default truncated Normal model (Eq. 14), which is again expected given that we do not model correlations among these parameters.

Assuming a scale-invariant prior on the merger rate, $\pi(\mathcal{R}_{\text{NSBH}}) \propto 1/\mathcal{R}_{\text{NSBH}}$, we infer an overall neutron star–black hole merger rate of $\mathcal{R}_{\text{NSBH}} = 104.3^{+118.3}_{-61.8} \text{ Gpc}^{-3} \text{ yr}^{-1}$, and $\mathcal{R}_{\text{NSBH}} = 92.2^{+123.4}_{-59.6} \text{ Gpc}^{-3} \text{ yr}^{-1}$ when restricting the analysis to quasi-circular binaries, as shown in Fig. 6. Including or excluding the eccentric event GW200105 has only a minimal impact on the inferred merger rate. These rates are broadly consistent with those reported in (A. G. Abac et al. 2024, 2025b), though we emphasise that these constraints remain limited by the small number of confidently identified NSBH mergers, and caution that individual events can disproportionately influence population-level inferences.

As a final caveat, our population model does not incorporate the full set of correlations that may exist among the hyperparameters. For simplicity, we assume that the masses, spins, and orbital eccentricities are independent at the population level, reducing the dimensionality of the hyperparameter space. However, most astrophysical formation scenarios naturally predict correlated structure in these parameters. For example, correlations between the mass ratio q and the effective inspiral spin χ_{eff} have been identified in the binary black hole population (T. A. Callister et al. 2021; C. Adamcewicz & E. Thrane 2022;

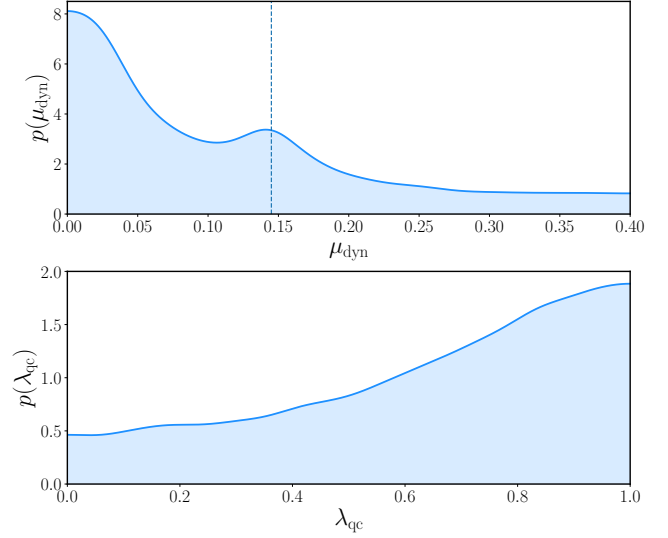


Figure 5. Select hyperposteriors for the truncated Normal mixture model, representing an eccentric (dynamical) channel and a quasi-circular (isolated) channel. The upper panel shows the population mean eccentricity of the dynamical component μ_{dyn} , exhibiting a mild peak near the value inferred for GW200105 (G. Morras et al. 2025a), denoted by the vertical dashed line. The lower panel displays the mixing fraction λ_{qc} between the two channels. This parameter is only weakly constrained, but does disfavor a purely dynamical population, consistent with event-level parameter estimation.

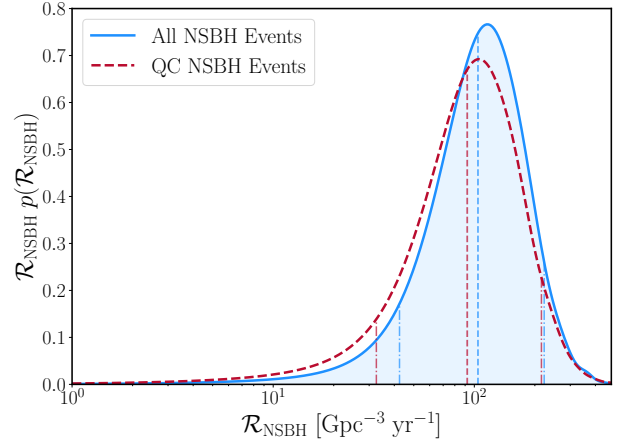


Figure 6. Merger rates for the NSBH population under two assumptions. First, that GW200105 is treated as part of a common NSBH population (blue). Second, that the orbital eccentricity observed in GW200105 suggests that it formed through a dynamical channel and should be treated separately and is excluded from the analysis (red, dashed). The vertical lines denote the median and 90% credible interval.

A. G. Abac et al. 2025b) and there is evidence that the spin distribution broadens with redshift (S. Biscoveanu et al. 2022a). Similar correlations involving eccentricity, spin-orbit misalignment, and component masses are expected, given our understanding of dynamical or triple-induced formation pathways (J. Stegmann & J. Klencki 2025).

Neglecting such correlations can influence hierarchical inference in several ways, due to model misspecification (E. Payne & E. Thrane 2023). Correlated subpopulations projected onto independent, marginalized one-dimensional distributions may artificially broaden the posteriors, while correlated features may mimic or obscure signatures associated with a particular formation channels. In turn, this can bias our inference on the branching ratios or mixing fractions. With only a handful of NSBH systems having been observed, the data cannot yet meaningfully constrain higher-dimensional correlated population models, and any inferred correlations would be poorly determined. Nevertheless, as the number of NSBH observations grows, incorporating correlated structures will become essential for accurate astrophysical inference.

5. CONCLUSIONS

We revisited the population properties of neutron star–black hole mergers using eccentric, precessing waveform analyses of all currently reported low-mass compact binary coalescences. Under a scale-invariant prior on the merger rate, we inferred consistent rates whether analysing the full sample or restricting to the quasi-circular subset, indicating that the overall rate estimate is not driven by the inclusion of the eccentric event GW200105.

Treating all NSBH mergers as a single population remains compatible with dynamically influenced formation channels. In particular, hierarchical triples naturally reproduce several qualitative features of the observed population (J. Stegmann & J. Klencki 2025), including measurable residual eccentricity and broad spin–orbit misalignment without requiring fine tuning.

At the same time, the quasi-circular subset shows no compelling deviations from expectations based on isolated binary evolution. Whilst there is a mild preference for $\cos\theta_{\text{BH}} < 0$, which would be in tension with the predictions from isolated evolution, we do not yet have enough information to make robust astrophysical statements or to decouple this from prior- and correlation-driven effects. The inferred eccentricities are consistent with efficient circularisation and the component masses fall within ranges compatible with standard field-binary formation. These systems may therefore represent a

subpopulation consistent with canonical isolated evolution (F. S. Broekgaarden et al. 2021).

The eccentricity observed in GW200105, however, cannot be reconciled with isolated evolution and must be accommodated for in any complete formation picture. This suggests either a single formation pathway capable of producing both quasi-circular and eccentric systems, or the presence of multiple subpopulations with distinct evolutionary origins. The current sample is too small to robustly discriminate between these possibilities, but it is already clear that field-binary evolution alone cannot account for the full diversity of observed NSBH mergers.

As of now, population-level conclusions on NSBH binaries remains limited by small-number statistics. Although GW230529 lowers the minimum black hole mass and GW200105 influences the inferred spin-magnitude distribution, the overall sample still favours comparatively low black hole spins and only weakly constrains spin–orbit orientations. Additional observations will be required to determine whether these trends persist, and to quantify the relative contributions of isolated and dynamical channels.

We have entered an exciting period of gravitational-wave astronomy, in which orbital eccentricity is starting to become a uniquely powerful tracer of compact-binary assembly. Unlike masses or spins, which can be degenerate across binary formation channels, measurable eccentricity in the LIGO–Virgo–KAGRA band offers a direct signature of dynamical formation in environments such as globular clusters, nuclear star clusters, hierarchical triples, or AGN disks, while isolated evolution predicts near-circular orbits by the time systems are detectable. As sensitivity improves, and the sample of events grows, joint population inference on rates, masses, spins, and eccentricity will enable far more definitive discrimination between these pathways, especially when correlations between these parameters are taken into account. This progress positions NSBH binaries as particularly valuable probes of the astrophysical conditions that shape compact binary mergers.

ACKNOWLEDGMENTS

The authors thank Reed Essick and Ivan Markin for useful comments on the manuscript. G.M. acknowledges support from the Ministerio de Universidades through Grants No. FPU20/02857 and No. EST24/00099, and from the Agencia Estatal de Investigación through the Grant IFT Centro de Excelencia Severo Ochoa No. CEX2020-001007-S, funded by MCIN/AEI/10.13039/501100011033. G.P. is very grate-

ful for support from a Royal Society University Research Fellowship URF\R1\221500 and RF\ERE\221015, and gratefully acknowledges support from an NVIDIA Academic Hardware Grant. G.P. and P.S. acknowledge support from STFC grants ST/V005677/1 and ST/Y00423X/1, and a UK Space Agency grant ST/Y004922/1. P.S. also acknowledges support from a Royal Society Research Grant RG\R1\241327. The authors are grateful to the Rates and Populations group in the LVK for preliminary feedback on the research. The authors are grateful for computational resources provided by the LIGO Laboratory (CIT) and supported by the National Science Foundation Grants PHY-0757058 and PHY-0823459, the University of Birmingham's BlueBEAR HPC service, which provides a High Performance Computing service to the University's research community, as well as resources provided by Supercomputing Wales, funded by STFC grants ST/I006285/1 and ST/V001167/1 supporting the UK Involvement in the Operation of Advanced LIGO. This research has made use of data or software obtained from the Gravitational Wave Open Science Center (gwosc.org), a service of the LIGO Scientific Collaboration, the Virgo Collaboration, and KAGRA. This material is based upon work supported by NSF's LIGO Laboratory which is a major facility fully funded by the National Science Foundation, as well as the Science and Technology Facilities Council (STFC) of the United Kingdom, the Max-Planck-Society (MPS), and the State of Niedersachsen/Germany for support of the construction of Advanced LIGO and construction and operation of the GEO600 detector. Additional support for Advanced LIGO was provided by the Australian Research Council. Virgo is funded, through the European Gravitational Observatory (EGO), by the French Centre National de Recherche Scientifique (CNRS), the Italian Istituto Nazionale di Fisica Nucleare (INFN) and the Dutch Nikhef, with contributions by institutions from Belgium, Germany, Greece, Hungary, Ireland, Japan, Monaco, Poland, Portugal, Spain. KAGRA is supported by Ministry of Education, Culture, Sports, Science and Technology (MEXT), Japan Society for the Promotion of Science (JSPS) in Japan; National Research Foundation (NRF) and Ministry of Science and ICT (MSIT) in Korea; Academia Sinica (AS) and National Science and Technology Council (NSTC) in Taiwan. Figures were prepared using `Matplotlib` (J. D. Hunter 2007). Analyses were performed using `Bilby` (G. Ashton et al. 2019a), `Dynesty` (J. S. Speagle 2020a), `LALSuite` (LIGO Scientific Collaboration et al. 2018), `NumPy` (C. R. Harris et al. 2020), `pyEFPE` (G. Morras et al. 2025b), and `Scipy` (P. Virtanen et al. 2020).

APPENDIX

A. PRIORS ON POPULATION HYPERPARAMETERS

Table 2. Prior ranges on the population hyperparameters describing the mass, spin, and eccentricity distributions used in our hierarchical Bayesian inference. All priors are taken to be uniform.

Symbol	Parameter	Minimum	Maximum
α	black hole mass power-law index	-4	12
$m_{\text{BH,min}}$	minimum black hole mass	$2 M_{\odot}$	$10 M_{\odot}$
$m_{\text{BH,max}}$	maximum black hole mass	$8 M_{\odot}$	$20 M_{\odot}$
$m_{\text{NS,max}}$	maximum neutron star mass	$1.97 M_{\odot}$	$2.7 M_{\odot}$
μ	mass ratio mean	0.1	0.6
σ	mass ratio standard deviation	0.1	1
α_{χ}	black hole spin α	0.1	8
β_{χ}	black hole spin β	0.1	8
μ_e	mean of eccentricity	0	0.4
σ_e	standard deviation of eccentricity	10^{-3}	0.5
μ_{dyn}	mean of eccentricity for the eccentric component of the mixture model	10^{-3}	0.5
σ_{dyn}	standard deviation of eccentricity for the eccentric component of the mixture model	10^{-3}	0.5
μ_{qc}	mean of eccentricity for the quasi-circular component of the mixture model	0	0
σ_{qc}	standard deviation of eccentricity for the quasi-circular component of the mixture model	10^{-3}	0.5
λ_{qc}	Mixing fraction between quasi-circular ($\lambda_{\text{qc}} = 1$) and eccentric ($\lambda_{\text{qc}} = 0$) populations	0	1

REFERENCES

- Aasi, J., et al. 2015, *Class. Quant. Grav.*, 32, 074001, doi: [10.1088/0264-9381/32/7/074001](https://doi.org/10.1088/0264-9381/32/7/074001)
- Abac, A. G., et al. 2024, *Astrophys. J. Lett.*, 970, L34, doi: [10.3847/2041-8213/ad5beb](https://doi.org/10.3847/2041-8213/ad5beb)
- Abac, A. G., et al. 2025a, <https://arxiv.org/abs/2508.18082>
- Abac, A. G., et al. 2025b, <https://arxiv.org/abs/2508.18083>
- Abbott, B. P., et al. 2017, *Phys. Rev. Lett.*, 119, 161101, doi: [10.1103/PhysRevLett.119.161101](https://doi.org/10.1103/PhysRevLett.119.161101)
- Abbott, B. P., et al. 2019a, *Phys. Rev. X*, 9, 031040, doi: [10.1103/PhysRevX.9.031040](https://doi.org/10.1103/PhysRevX.9.031040)
- Abbott, B. P., et al. 2019b, *Phys. Rev. X*, 9, 011001, doi: [10.1103/PhysRevX.9.011001](https://doi.org/10.1103/PhysRevX.9.011001)
- Abbott, B. P., et al. 2020, *Astrophys. J. Lett.*, 892, L3, doi: [10.3847/2041-8213/ab75f5](https://doi.org/10.3847/2041-8213/ab75f5)
- Abbott, R., et al. 2020, *Astrophys. J. Lett.*, 896, L44, doi: [10.3847/2041-8213/ab960f](https://doi.org/10.3847/2041-8213/ab960f)
- Abbott, R., et al. 2021a, *Astrophys. J. Lett.*, 915, L5, doi: [10.3847/2041-8213/ac082e](https://doi.org/10.3847/2041-8213/ac082e)
- Abbott, R., et al. 2021b, *Phys. Rev. X*, 11, 021053, doi: [10.1103/PhysRevX.11.021053](https://doi.org/10.1103/PhysRevX.11.021053)
- Abbott, R., et al. 2021c, *SoftwareX*, 13, 100658, doi: [10.1016/j.softx.2021.100658](https://doi.org/10.1016/j.softx.2021.100658)
- Abbott, R., et al. 2021d, doi: [10.5281/zenodo.5636816](https://doi.org/10.5281/zenodo.5636816)
- Abbott, R., et al. 2023a, *Phys. Rev. X*, 13, 041039, doi: [10.1103/PhysRevX.13.041039](https://doi.org/10.1103/PhysRevX.13.041039)
- Abbott, R., et al. 2023b, *Astrophys. J. Suppl.*, 267, 29, doi: [10.3847/1538-4365/acdc9f](https://doi.org/10.3847/1538-4365/acdc9f)
- Abbott, R., et al. 2023c, *Phys. Rev. X*, 13, 011048, doi: [10.1103/PhysRevX.13.011048](https://doi.org/10.1103/PhysRevX.13.011048)
- Abbott, R., et al. 2024, *Phys. Rev. D*, 109, 022001, doi: [10.1103/PhysRevD.109.022001](https://doi.org/10.1103/PhysRevD.109.022001)
- Acernese, F., et al. 2015, *Class. Quant. Grav.*, 32, 024001, doi: [10.1088/0264-9381/32/2/024001](https://doi.org/10.1088/0264-9381/32/2/024001)
- Adamcewicz, C., & Thrane, E. 2022, *Mon. Not. Roy. Astron. Soc.*, 517, 3928, doi: [10.1093/mnras/stac2961](https://doi.org/10.1093/mnras/stac2961)
- Ajith, P., et al. 2011, *Phys. Rev. Lett.*, 106, 241101, doi: [10.1103/PhysRevLett.106.241101](https://doi.org/10.1103/PhysRevLett.106.241101)
- Akutsu, T., et al. 2021, *PTEP*, 2021, 05A101, doi: [10.1093/ptep/ptaa125](https://doi.org/10.1093/ptep/ptaa125)
- Antonini, F., Toonen, S., & Hamers, A. S. 2017, *Astrophys. J.*, 841, 77, doi: [10.3847/1538-4357/aa6f5e](https://doi.org/10.3847/1538-4357/aa6f5e)
- Ashton, G., et al. 2019a, *Astrophys. J. Suppl.*, 241, 27, doi: [10.3847/1538-4365/ab06fc](https://doi.org/10.3847/1538-4365/ab06fc)
- Ashton, G., et al. 2019b, *Astrophys. J. Suppl.*, 241, 27, doi: [10.3847/1538-4365/ab06fc](https://doi.org/10.3847/1538-4365/ab06fc)
- Belczynski, K., Kalogera, V., & Bulik, T. 2001, *Astrophys. J.*, 572, 407, doi: [10.1086/340304](https://doi.org/10.1086/340304)
- Biscoveanu, S., Callister, T. A., Haster, C.-J., et al. 2022a, *Astrophys. J. Lett.*, 932, L19, doi: [10.3847/2041-8213/ac71a8](https://doi.org/10.3847/2041-8213/ac71a8)
- Biscoveanu, S., Landry, P., & Vitale, S. 2022b, *Mon. Not. Roy. Astron. Soc.*, 518, 5298, doi: [10.1093/mnras/stac3052](https://doi.org/10.1093/mnras/stac3052)
- Brandt, N., & Podsiadlowski, P. 1995, *MNRAS*, 274, 461, doi: [10.1093/mnras/274.2.461](https://doi.org/10.1093/mnras/274.2.461)
- Broekgaarden, F. S., & Berger, E. 2021, *Astrophys. J. Lett.*, 920, L13, doi: [10.3847/2041-8213/ac2832](https://doi.org/10.3847/2041-8213/ac2832)
- Broekgaarden, F. S., Berger, E., Neijssel, C. J., et al. 2021, *Mon. Not. Roy. Astron. Soc.*, 508, 5028, doi: [10.1093/mnras/stab2716](https://doi.org/10.1093/mnras/stab2716)
- Buikema, A., et al. 2020, *Phys. Rev. D*, 102, 062003, doi: [10.1103/PhysRevD.102.062003](https://doi.org/10.1103/PhysRevD.102.062003)
- Cabero, M., Nielsen, A. B., Lundgren, A. P., & Capano, C. D. 2017, *Phys. Rev. D*, 95, 064016, doi: [10.1103/PhysRevD.95.064016](https://doi.org/10.1103/PhysRevD.95.064016)
- Callister, T. A. 2024, <https://arxiv.org/abs/2410.19145>
- Callister, T. A., Haster, C.-J., Ng, K. K. Y., Vitale, S., & Farr, W. M. 2021, *Astrophys. J. Lett.*, 922, L5, doi: [10.3847/2041-8213/ac2ccc](https://doi.org/10.3847/2041-8213/ac2ccc)
- Capote, E., et al. 2025, *Phys. Rev. D*, 111, 062002, doi: [10.1103/PhysRevD.111.062002](https://doi.org/10.1103/PhysRevD.111.062002)
- Chatziioannou, K., Cornish, N., Klein, A., & Yunes, N. 2015, *Astrophys. J. Lett.*, 798, L17, doi: [10.1088/2041-8205/798/1/L17](https://doi.org/10.1088/2041-8205/798/1/L17)
- Cornish, N. J., & Littenberg, T. B. 2015, *Class. Quant. Grav.*, 32, 135012, doi: [10.1088/0264-9381/32/13/135012](https://doi.org/10.1088/0264-9381/32/13/135012)
- Cornish, N. J., Littenberg, T. B., Bécsy, B., et al. 2021, *Phys. Rev. D*, 103, 044006, doi: [10.1103/PhysRevD.103.044006](https://doi.org/10.1103/PhysRevD.103.044006)
- Cutler, C., & Flanagan, E. E. 1994, *Phys. Rev. D*, 49, 2658, doi: [10.1103/PhysRevD.49.2658](https://doi.org/10.1103/PhysRevD.49.2658)
- Damour, T. 2001, *Phys. Rev. D*, 64, 124013, doi: [10.1103/PhysRevD.64.124013](https://doi.org/10.1103/PhysRevD.64.124013)
- Dhurkunde, R., & Nitz, A. H. 2025, *Phys. Rev. D*, 111, 103018, doi: [10.1103/PhysRevD.111.103018](https://doi.org/10.1103/PhysRevD.111.103018)
- Dorozsmai, A., Romero-Shaw, I. M., Vijaykumar, A., et al. 2025, *Mon. Not. Roy. Astron. Soc.*, 545, staf1938, doi: [10.1093/mnras/staf1938](https://doi.org/10.1093/mnras/staf1938)
- Drozda, P., Belczynski, K., O’Shaughnessy, R., Bulik, T., & Fryer, C. L. 2022, *Astron. Astrophys.*, 667, A126, doi: [10.1051/0004-6361/202039418](https://doi.org/10.1051/0004-6361/202039418)
- Essick, R. 2026, *Astrophys. J.*, 997, 76, doi: [10.3847/1538-4357/ae2255](https://doi.org/10.3847/1538-4357/ae2255)
- Fan, Y.-Z., Han, M.-Z., Jiang, J.-L., Shao, D.-S., & Tang, S.-P. 2024, *Phys. Rev. D*, 109, 043052, doi: [10.1103/PhysRevD.109.043052](https://doi.org/10.1103/PhysRevD.109.043052)

- Farah, A. M., Fishbach, M., Essick, R., Holz, D. E., & Galaudage, S. 2022, *Astrophys. J.*, 931, 108, doi: [10.3847/1538-4357/ac5f03](https://doi.org/10.3847/1538-4357/ac5f03)
- Farr, W. M. 2019, *Res. Notes AAS*, 3, 66, doi: [10.3847/2515-5172/ab1d5f](https://doi.org/10.3847/2515-5172/ab1d5f)
- Fishbach, M., & Holz, D. E. 2020, *Astrophys. J. Lett.*, 891, L27, doi: [10.3847/2041-8213/ab7247](https://doi.org/10.3847/2041-8213/ab7247)
- Flanagan, E. E., & Hinderer, T. 2008, *Phys. Rev. D*, 77, 021502, doi: [10.1103/PhysRevD.77.021502](https://doi.org/10.1103/PhysRevD.77.021502)
- Fragione, G., & Banerjee, S. 2020, *Astrophys. J. Lett.*, 901, L16, doi: [10.3847/2041-8213/abb671](https://doi.org/10.3847/2041-8213/abb671)
- Fragione, G., & Loeb, A. 2019, *Mon. Not. Roy. Astron. Soc.*, 486, 4443, doi: [10.1093/mnras/stz1131](https://doi.org/10.1093/mnras/stz1131)
- Fragione, G., Loeb, A., & Rasio, F. A. 2021, *Astrophys. J. Lett.*, 918, L38, doi: [10.3847/2041-8213/ac225a](https://doi.org/10.3847/2041-8213/ac225a)
- Freire, P. C. C., et al. 2004, *Astrophys. J. Lett.*, 606, L53, doi: [10.1086/421085](https://doi.org/10.1086/421085)
- Fuller, J., & Ma, L. 2019, *Astrophys. J. Lett.*, 881, L1, doi: [10.3847/2041-8213/ab339b](https://doi.org/10.3847/2041-8213/ab339b)
- García-Quirós, C., Colleoni, M., Husa, S., et al. 2020, *Phys. Rev. D*, 102, 064002, doi: [10.1103/PhysRevD.102.064002](https://doi.org/10.1103/PhysRevD.102.064002)
- Giacobbo, N., & Mapelli, M. 2019, doi: [10.3847/1538-4357/ab7335](https://doi.org/10.3847/1538-4357/ab7335)
- Gupte, N., et al. 2025, *Phys. Rev. D*, 112, 104045, doi: [10.1103/vpyp-nvfp](https://doi.org/10.1103/vpyp-nvfp)
- Hamers, A. S., & Thompson, T. A. 2019, doi: [10.3847/1538-4357/ab3b06](https://doi.org/10.3847/1538-4357/ab3b06)
- Harris, C. R., et al. 2020, *Nature*, 585, 357, doi: [10.1038/s41586-020-2649-2](https://doi.org/10.1038/s41586-020-2649-2)
- Harry, I., & Hinderer, T. 2018, *Class. Quant. Grav.*, 35, 145010, doi: [10.1088/1361-6382/aac7e3](https://doi.org/10.1088/1361-6382/aac7e3)
- Hoang, B.-M., Naoz, S., & Kremer, K. 2020, *Astrophys. J.*, 903, 8, doi: [10.3847/1538-4357/abb66a](https://doi.org/10.3847/1538-4357/abb66a)
- Hunter, J. D. 2007, *Computing In Science & Engineering*, 9, 90
- Jan, A., Tsao, B.-J., O’Shaughnessy, R., Shoemaker, D., & Laguna, P. 2026, *Phys. Rev. D*, 113, 024018, doi: [10.1103/zjmc-117s](https://doi.org/10.1103/zjmc-117s)
- Kacanja, K., Soni, K., & Nitz, A. H. 2025, *Phys. Rev. D*, 112, 122007, doi: [10.1103/jnsc-783p](https://doi.org/10.1103/jnsc-783p)
- Kalogera, V. 1996, *Astrophys. J.*, 471, 352, doi: [10.1086/177974](https://doi.org/10.1086/177974)
- Kalogera, V. 2000, *Astrophys. J.*, 541, 319, doi: [10.1086/309400](https://doi.org/10.1086/309400)
- Kiziltan, B., Kottas, A., De Yoreo, M., & Thorsett, S. E. 2013, *Astrophys. J.*, 778, 66, doi: [10.1088/0004-637X/778/1/66](https://doi.org/10.1088/0004-637X/778/1/66)
- Kozai, Y. 1962, *Astron. J.*, 67, 591, doi: [10.1086/108790](https://doi.org/10.1086/108790)
- Kushnir, D., Zaldarriaga, M., Kollmeier, J. A., & Waldman, R. 2016, *Mon. Not. Roy. Astron. Soc.*, 462, 844, doi: [10.1093/mnras/stw1684](https://doi.org/10.1093/mnras/stw1684)
- Landry, P., & Read, J. S. 2021, *Astrophys. J. Lett.*, 921, L25, doi: [10.3847/2041-8213/ac2f3e](https://doi.org/10.3847/2041-8213/ac2f3e)
- Lenon, A. K., Nitz, A. H., & Brown, D. A. 2020, *Mon. Not. Roy. Astron. Soc.*, 497, 1966, doi: [10.1093/mnras/staa2120](https://doi.org/10.1093/mnras/staa2120)
- Lidov, M. L. 1962, *Planet. Space Sci.*, 9, 719, doi: [10.1016/0032-0633\(62\)90054-3](https://doi.org/10.1016/0032-0633(62)90054-3)
- LIGO Scientific Collaboration, Virgo Collaboration, & KAGRA Collaboration. 2018,, Free software (GPL) doi: [10.7935/GT1W-FZ16](https://doi.org/10.7935/GT1W-FZ16)
- LIGO-Virgo Collaboration. 2017,, LIGO Open Science Center <https://doi.org/10.7935/K5B8566F>
- Loredo, T. J. 2004, *AIP Conf. Proc.*, 735, 195, doi: [10.1063/1.1835214](https://doi.org/10.1063/1.1835214)
- LVK Collaboration. 2020a,, Technical Report LIGO-T1900685-v1, LIGO Scientific Collaboration, Pasadena, CA, USA
- LVK Collaboration. 2020b,, Technical Report LIGO-P2000026-v2, LIGO Scientific Collaboration, Pasadena, CA, USA
- LVK Collaboration. 2020c,, Technical Report LIGO-P2000223-v7, LIGO Scientific Collaboration, Pasadena, CA, USA
- LVK Collaboration. 2021,, Zenodo, version 1 doi: [10.5281/zenodo.5546680](https://doi.org/10.5281/zenodo.5546680)
- LVK Collaboration. 2022,, Zenodo, version 2 doi: [10.5281/zenodo.6513631](https://doi.org/10.5281/zenodo.6513631)
- LVK Collaboration. 2023a,, Zenodo, version 2 doi: [10.5281/zenodo.8177023](https://doi.org/10.5281/zenodo.8177023)
- LVK Collaboration. 2023b, doi: [10.7935/6k89-7q62](https://doi.org/10.7935/6k89-7q62)
- Mandel, I., Farr, W. M., & Gair, J. R. 2019, *Mon. Not. Roy. Astron. Soc.*, 486, 1086, doi: [10.1093/mnras/stz896](https://doi.org/10.1093/mnras/stz896)
- Mandel, I., & Fragos, T. 2020, *Astrophys. J. Lett.*, 895, L28, doi: [10.3847/2041-8213/ab8e41](https://doi.org/10.3847/2041-8213/ab8e41)
- Mandel, I., & Smith, R. J. E. 2021, *Astrophys. J. Lett.*, 922, L14, doi: [10.3847/2041-8213/ac35dd](https://doi.org/10.3847/2041-8213/ac35dd)
- Mapelli, M., & Giacobbo, N. 2018, *Mon. Not. Roy. Astron. Soc.*, 479, 4391, doi: [10.1093/mnras/sty1613](https://doi.org/10.1093/mnras/sty1613)
- Margalit, B., & Metzger, B. D. 2017, *Astrophys. J. Lett.*, 850, L19, doi: [10.3847/2041-8213/aa991c](https://doi.org/10.3847/2041-8213/aa991c)
- McKernan, B., Ford, K. E. S., & O’Shaughnessy, R. 2020, *Mon. Not. Roy. Astron. Soc.*, 498, 4088, doi: [10.1093/mnras/staa2681](https://doi.org/10.1093/mnras/staa2681)
- Michaely, E., & Naoz, S. 2022, *Astrophys. J.*, 936, 184, doi: [10.3847/1538-4357/ac8a92](https://doi.org/10.3847/1538-4357/ac8a92)
- Moe, M., & Di Stefano, R. 2017, *ApJS*, 230, 15, doi: [10.3847/1538-4365/aa6fb6](https://doi.org/10.3847/1538-4365/aa6fb6)

- Morras, G., Pratten, G., & Schmidt, P. 2025a, <https://arxiv.org/abs/2503.15393>
- Morras, G., Pratten, G., & Schmidt, P. 2025b, *Phys. Rev. D*, 111, 084052, doi: [10.1103/PhysRevD.111.084052](https://doi.org/10.1103/PhysRevD.111.084052)
- Most, E. R., Papenfort, L. J., Weih, L. R., & Rezzolla, L. 2020, *Mon. Not. Roy. Astron. Soc.*, 499, L82, doi: [10.1093/mnras/laa168](https://doi.org/10.1093/mnras/laa168)
- Nitz, A. H., & Wang, Y.-F. 2021, *Astrophys. J.*, 915, 54, doi: [10.3847/1538-4357/ac01d9](https://doi.org/10.3847/1538-4357/ac01d9)
- Oh, M., Fishbach, M., Kimball, C., Kalogera, V., & Ye, C. 2023, *Astrophys. J.*, 953, 152, doi: [10.3847/1538-4357/ace349](https://doi.org/10.3847/1538-4357/ace349)
- Payne, E., & Thrane, E. 2023, *Phys. Rev. Res.*, 5, 023013, doi: [10.1103/PhysRevResearch.5.023013](https://doi.org/10.1103/PhysRevResearch.5.023013)
- Peters, P. C. 1964, *Phys. Rev.*, 136, B1224, doi: [10.1103/PhysRev.136.B1224](https://doi.org/10.1103/PhysRev.136.B1224)
- Phukon, K. S., Schmidt, P., Morras, G., & Pratten, G. 2025a, <https://arxiv.org/abs/2512.10803>
- Phukon, K. S., Schmidt, P., & Pratten, G. 2025b, *Phys. Rev. D*, 111, 043040, doi: [10.1103/PhysRevD.111.043040](https://doi.org/10.1103/PhysRevD.111.043040)
- Planas, M. d. L., Husa, S., Ramos-Buades, A., & Valencia, J. 2025a, *Astrophys. J.*, 995, 47, doi: [10.3847/1538-4357/ae1d7d](https://doi.org/10.3847/1538-4357/ae1d7d)
- Planas, M. d. L., Ramos-Buades, A., García-Quirós, C., et al. 2025b, *Phys. Rev. D*, 112, 123004, doi: [10.1103/cv75-y8dr](https://doi.org/10.1103/cv75-y8dr)
- Portegies Zwart, S. F., & McMillan, S. 2000, *Astrophys. J. Lett.*, 528, L17, doi: [10.1086/312422](https://doi.org/10.1086/312422)
- Pratten, G., Husa, S., Garcia-Quiros, C., et al. 2020a, *Phys. Rev. D*, 102, 064001, doi: [10.1103/PhysRevD.102.064001](https://doi.org/10.1103/PhysRevD.102.064001)
- Pratten, G., Schmidt, P., Buscicchio, R., & Thomas, L. M. 2020b, *Phys. Rev. Res.*, 2, 043096, doi: [10.1103/PhysRevResearch.2.043096](https://doi.org/10.1103/PhysRevResearch.2.043096)
- Pratten, G., Schmidt, P., & Williams, N. 2022, *Phys. Rev. Lett.*, 129, 081102, doi: [10.1103/PhysRevLett.129.081102](https://doi.org/10.1103/PhysRevLett.129.081102)
- Pratten, G., et al. 2021, *Phys. Rev. D*, 103, 104056, doi: [10.1103/PhysRevD.103.104056](https://doi.org/10.1103/PhysRevD.103.104056)
- Qin, Y., Fragos, T., Meynet, G., et al. 2018, *Astron. Astrophys.*, 616, A28, doi: [10.1051/0004-6361/201832839](https://doi.org/10.1051/0004-6361/201832839)
- Racine, E. 2008, *Phys. Rev. D*, 78, 044021, doi: [10.1103/PhysRevD.78.044021](https://doi.org/10.1103/PhysRevD.78.044021)
- Rastello, S., et al. 2020, *Mon. Not. Roy. Astron. Soc.*, 497, 1563, doi: [10.1093/mnras/staa2018](https://doi.org/10.1093/mnras/staa2018)
- Rezzolla, L., Most, E. R., & Weih, L. R. 2018, *Astrophys. J. Lett.*, 852, L25, doi: [10.3847/2041-8213/aaa401](https://doi.org/10.3847/2041-8213/aaa401)
- Rocha, K. A., et al. 2025, *Astrophys. J.*, 983, 39, doi: [10.3847/1538-4357/adb970](https://doi.org/10.3847/1538-4357/adb970)
- Rodriguez, C. L., & Antonini, F. 2018, *Astrophys. J.*, 863, 7, doi: [10.3847/1538-4357/aacea4](https://doi.org/10.3847/1538-4357/aacea4)
- Rodriguez, C. L., Zevin, M., Pankow, C., Kalogera, V., & Rasio, F. A. 2016, *Astrophys. J. Lett.*, 832, L2, doi: [10.3847/2041-8205/832/1/L2](https://doi.org/10.3847/2041-8205/832/1/L2)
- Romero-Shaw, I., Stegmann, J., Morras, G., Dorozsmai, A., & Zevin, M. 2025, <https://arxiv.org/abs/2512.16289>
- Romero-Shaw, I. M., Lasky, P. D., & Thrane, E. 2022, *Astrophys. J.*, 940, 171, doi: [10.3847/1538-4357/ac9798](https://doi.org/10.3847/1538-4357/ac9798)
- Schmidt, P., Hannam, M., Husa, S., & Ajith, P. 2011, *Phys. Rev. D*, 84, 024046, doi: [10.1103/PhysRevD.84.024046](https://doi.org/10.1103/PhysRevD.84.024046)
- Schmidt, P., Ohme, F., & Hannam, M. 2015, *Phys. Rev. D*, 91, 024043, doi: [10.1103/PhysRevD.91.024043](https://doi.org/10.1103/PhysRevD.91.024043)
- Sedda, M. A. 2020, *Commun. Phys.*, 3, 43, doi: [10.1038/s42005-020-0310-x](https://doi.org/10.1038/s42005-020-0310-x)
- Shao, D.-S., Tang, S.-P., Sheng, X., et al. 2020, *Phys. Rev. D*, 101, 063029, doi: [10.1103/PhysRevD.101.063029](https://doi.org/10.1103/PhysRevD.101.063029)
- Shibata, M., Zhou, E., Kiuchi, K., & Fujibayashi, S. 2019, *Phys. Rev. D*, 100, 023015, doi: [10.1103/PhysRevD.100.023015](https://doi.org/10.1103/PhysRevD.100.023015)
- Silsbee, K., & Tremaine, S. 2017, *Astrophys. J.*, 836, 39, doi: [10.3847/1538-4357/aa5729](https://doi.org/10.3847/1538-4357/aa5729)
- Singh, M. K., Patterson, B. G., & Fairhurst, S. 2025, <https://arxiv.org/abs/2512.07688>
- Skilling, J. 2006, *Bayesian Analysis*, 1, 833, doi: [10.1214/06-BA127](https://doi.org/10.1214/06-BA127)
- Speagle, J. S. 2020a, *Monthly Notices of the Royal Astronomical Society*, 493, 3132, doi: [10.1093/mnras/staa278](https://doi.org/10.1093/mnras/staa278)
- Speagle, J. S. 2020b, *Mon. Not. Roy. Astron. Soc.*, 493, 3132, doi: [10.1093/mnras/staa278](https://doi.org/10.1093/mnras/staa278)
- Stegmann, J., Antonini, F., Olejak, A., et al. 2025a, <https://arxiv.org/abs/2512.15873>
- Stegmann, J., Gerosa, D., Romero-Shaw, I., et al. 2025b, *Astrophys. J. Lett.*, 994, L47, doi: [10.3847/2041-8213/ae1d66](https://doi.org/10.3847/2041-8213/ae1d66)
- Stegmann, J., & Klencki, J. 2025, *Astrophys. J. Lett.*, 991, L54, doi: [10.3847/2041-8213/ae055b](https://doi.org/10.3847/2041-8213/ae055b)
- Stegmann, J., Vigna-Gómez, A., Rantala, A., et al. 2024, *Astrophys. J. Lett.*, 972, L19, doi: [10.3847/2041-8213/ad70bb](https://doi.org/10.3847/2041-8213/ad70bb)
- Stone, N. C., Metzger, B. D., & Haiman, Z. 2017, *Mon. Not. Roy. Astron. Soc.*, 464, 946, doi: [10.1093/mnras/stw2260](https://doi.org/10.1093/mnras/stw2260)
- Talbot, C., Smith, R., Thrane, E., & Poole, G. B. 2019, *Phys. Rev. D*, 100, 043030, doi: [10.1103/PhysRevD.100.043030](https://doi.org/10.1103/PhysRevD.100.043030)
- Talbot, C., & Thrane, E. 2017, *Phys. Rev. D*, 96, 023012, doi: [10.1103/PhysRevD.96.023012](https://doi.org/10.1103/PhysRevD.96.023012)
- Tauris, T. M., et al. 2017, *Astrophys. J.*, 846, 170, doi: [10.3847/1538-4357/aa7e89](https://doi.org/10.3847/1538-4357/aa7e89)
- Thrane, E., & Talbot, C. 2019, *Publ. Astron. Soc. Austral.*, 36, e010, doi: [10.1017/pasa.2019.2](https://doi.org/10.1017/pasa.2019.2)

- Tiwari, A., Bhat, S. A., Shaikh, M. A., & Kapadia, S. J. 2025, *Astrophys. J.*, 995, 48, doi: [10.3847/1538-4357/ae1d74](https://doi.org/10.3847/1538-4357/ae1d74)
- Trani, A. A., et al. 2022, *Mon. Not. Roy. Astron. Soc.*, 511, 1362, doi: [10.1093/mnras/stac122](https://doi.org/10.1093/mnras/stac122)
- Van den Heuvel, E., & Yoon, S.-C. 2007, *Astrophysics and Space Science*, 311, 177
- Vecchio, A. 2004, *Phys. Rev. D*, 70, 042001, doi: [10.1103/PhysRevD.70.042001](https://doi.org/10.1103/PhysRevD.70.042001)
- Veitch, J., et al. 2015, *Phys. Rev. D*, 91, 042003, doi: [10.1103/PhysRevD.91.042003](https://doi.org/10.1103/PhysRevD.91.042003)
- Vigna-Gómez, A. 2025, *Astron. Astrophys.*, 701, L3, doi: [10.1051/0004-6361/202556051](https://doi.org/10.1051/0004-6361/202556051)
- Virtanen, P., et al. 2020, *Nature Methods*, 17, 261, doi: [10.1038/s41592-019-0686-2](https://doi.org/10.1038/s41592-019-0686-2)
- Vitale, S., Biscoveanu, S., & Talbot, C. 2022, *Astron. Astrophys.*, 668, L2, doi: [10.1051/0004-6361/202245084](https://doi.org/10.1051/0004-6361/202245084)
- von Zeipel, H. 1910, *Astron. Nachr.*, 183, 34, doi: [10.1002/asna.19101830302](https://doi.org/10.1002/asna.19101830302)
- Wysocki, D., Lange, J., & O’Shaughnessy, R. 2019, *Phys. Rev. D*, 100, 043012, doi: [10.1103/PhysRevD.100.043012](https://doi.org/10.1103/PhysRevD.100.043012)
- Wysocki, D., et al. 2018, *Phys. Rev. D*, 97, 043014, doi: [10.1103/PhysRevD.97.043014](https://doi.org/10.1103/PhysRevD.97.043014)
- Xing, Z., et al. 2024, *Astron. Astrophys.*, 683, A144, doi: [10.1051/0004-6361/202347971](https://doi.org/10.1051/0004-6361/202347971)
- Xu, Y., et al. 2025, <https://arxiv.org/abs/2512.19513>
- Yang, Y., Gayathri, V., Bartos, I., et al. 2020, *Astrophys. J. Lett.*, 901, L34, doi: [10.3847/2041-8213/abb940](https://doi.org/10.3847/2041-8213/abb940)
- Ye, C., & Fishbach, M. 2022, *Astrophys. J.*, 937, 73, doi: [10.3847/1538-4357/ac7f99](https://doi.org/10.3847/1538-4357/ac7f99)
- Ye, C. S., et al. 2019, *Astrophys. J.*, 877, 122, doi: [10.3847/1538-4357/ab1b21](https://doi.org/10.3847/1538-4357/ab1b21)
- Zeeshan, M., O’Shaughnessy, R., & Malagon, N. 2026, <https://arxiv.org/abs/2602.11030>
- Zenati, Y., Rozner, M., Krolik, J. H., & Most, E. R. 2025, *Astrophys. J.*, 978, 126, doi: [10.3847/1538-4357/ad9b87](https://doi.org/10.3847/1538-4357/ad9b87)
- Zevin, M., Samsing, J., Rodriguez, C., Haster, C.-J., & Ramirez-Ruiz, E. 2019, *Astrophys. J.*, 871, 91, doi: [10.3847/1538-4357/aaf6ec](https://doi.org/10.3847/1538-4357/aaf6ec)
- Zhu, J.-P., Wu, S., Qin, Y., et al. 2022, *Astrophys. J.*, 928, 167, doi: [10.3847/1538-4357/ac540c](https://doi.org/10.3847/1538-4357/ac540c)